Stevens Goddard, A.L., and Fosdick J.C., 2019, Multichronometer thermochronologic modeling of migrating spreading ridge subduction in southern Patagonia: Geology, https://doi.org/10.1130/G46091.1

GSA Data Repository Item 2019203

Data Repository

Tables
DR1. New (U-Th)/He and fission track thermochronology data.
DR2. Coded thermal modeling results and timing of onset of cooling (t_{cool}). This table shows all samples with data from > 1 thermochronometer. Modeling was attempted for all samples meeting this criteria. The coded results from the models in Figure DR2 are shown in the section of the table, 'Thermal Model Data', and include the range of acceptable modeled inflection points as constrained by the thermochronology data MAX t_{cool}, MEAN t_{cool}, and MIN t_{cool} derived from Figure DR2. If samples record a change in Neogene cooling rate *after* the change documented by the acceleration in cooling (tcool), we denote this with YES/NO/MAYBE (Y/N/M) in the column 'Neogene change in cooling rate'. The columns after this designate whether this change was an INCREASE/DECREASE (I/D) in column 'Neogene Cooling Increase or Decrease' and show the timing of this change in the columns 'Max onset change in cooling' and 'Min onset change in cooling'.

Figure
DR1. A) t_{cool} vs. trench distance; B) t_{cool} vs. longitude; C) sample elevation vs. t_{cool}
DR2. HeFTy inverse modeling results and example of coded outputs from HeFTy thermal models.

Extended Methods
Three new samples were collected and analyzed using three low-temperature thermochronology dating techniques, (U-Th-Sm)/He thermochronology on apatite and zircon (AHe, ZHe) and apatite fission track thermochronology (AFT). We specifically targeted collecting of new samples from the hinterland and thrust belt domains as these regions were underrepresented south of 52°S. Samples (1-2 kg) were collected at outcrops exposed near sea level in Seno Skyring accessed by zodiac watercraft. Samples FPT17-68 and FPT17-59 were collected for ZHe, AFT, and AHe from the Jurassic Tobífera Formation in the hinterland domain. One granitic conglomerate clast, FPT17-45 was collected in the thrust belt domain from the Upper Cretaceous Escarpada Formation for AFT and AHe thermochronology.

We integrated our new data with all existing thermochronology samples from the ZHe, AFT, and AHe systems published in the literature between 47° and 54° S (Figure 1; Thomson et al., 2001; 2010; Haschke et al., 2006; Fosdick et al., 2013; Guillaume et al., 2013; Georgieva et al., 2016; Christeleit et al., 2017). Zircon fission track (ZFT) data were omitted from this compendium as published ZFT dates have Late Cretaceous - Paleocene dates reflecting and earlier cooling history than the target of this study. All samples (55) with data from >2 thermochronometric systems (ZHe, AFT, and AHe) were chosen for thermal modeling (Table DR2).

(U-Th-Sm)/He thermochronology

Apatite and zircon grains were picked for (U-Th-Sm)/He thermochronology at the Basin Analysis and Helium Thermochronology Lab at the University of Connecticut. Whole euhedral grains were selected for clarity and size using a Leica M165 binocular microscope. Single grain aliquots were secured in Nb tubes. For each sample, four grains were analyzed for ZHe thermochronology and three grains were analyzed for AHe thermochronology at the University of Colorado Thermochronology Research and Instrumentation Lab (TRaIL). Nb-packed aliquots were loaded in an ASI AlphachronTM to extract and measure He gas. A 25W diode laser heated the aliquot to ca. 800-110°C for 5 to 10 minutes to extract 4He gas. A spike of 13 ncc ^{3}He was used to spike extracted ^{4}He gas and analyzed on a Balzers PrismaPlus QME 220 quadrupole mass spectrometer. Apatite grains and Nb tubes are dissolved in HNO_3 spiked with a ^{235}U, ^{230}Th, ^{145}Nd tracer. Zircon grains and niobium tubes are dissolved in a series of HF solutions - the first spiked with a ^{235}U, ^{230}Th, ^{145}Nd tracer - and a final HNO_3:HF mixture. Both apatite and zircon samples solutions are analyzed for U, Th and Sm on a Thermo Element 2 magnetic sector ICP-MS. Results are reported in Table DR1.

Apatite Fission Track Thermochronology

Apatite fission track samples were prepared following the methods of Donelick et al. (2005) by mounting apatite grains in epoxy, polishing the mounts, and etching samples with 5.5M nitric acid for 20 seconds at 21°C. A mica sheet was affixed to the epoxy mount and irradiated at Oregon State University. Upon return from the reactor, the mica sheets were etched in 49% HF for ~ 15 minutes at 23°C. Apatite fission track thermochronology was conducted at the University of Arizona Fission Track Laboratory using the external detector method using 1600x magnification. Both track density ratios and average track etch pit diameter (D_{par}) was recorded for between 24 and 30 grains per sample. Results are reported in Table DR1.

Inverse Thermal Modeling

Results from ZHe, AFT, and AHe from new and existing data sets were modeled using HeFTy v.1.9.3 (Ketcham, 2005). For ZHe samples (using all grains available from our data and published data), we entered single grain data individually applying the helium diffusion model from Guenthner et al., (2013) and the ejection correction for alpha calculation. For a given sample, all available single-grain AHe dates were modeled together using the radiation damage accumulation and annealing model from Flowers et al., (2013) and the ejection correction for alpha calculation. Raw counting ratios were entered for AFT samples along with D_{par} measurements, when available. We used the apatite fission track annealing model from Ketcham et al., (2007).

Inverse model constraints for the 100 to 0 Ma time period were left purposely broad to explore all cooling histories, with constraints only at model initiation (100 and 300 °C between 80 and 50 Ma) and modern surface temperatures of 10 ± 5 °C. These constraints were designed to be consistent with four existing thermal models generated by Fosdick et al. (2013) using the inverse modeling tool in HeFTy from samples in the hinterland and internal thrust belt domains between 51° and 51.5° S. Although the model parameters described above explore only monotonic t-T paths, preliminary use of alternative model parameters that allow reheating failed to identify evidence of non-monotonic t-T paths. Each model was required to explore possible t-T paths until 100 paths with a goodness of fit >0.5 were identified.

Models were initially run with analytical error from ZHe, AFT, and AHe analyses; however, in 22/54 cases, models with these parameters failed to yield any t-T paths with a goodness of fit > 0.5 after exploring >100,000 t-T paths. In this case, it is reasonable to assume that there is additional error not due to analytical uncertainty, but from variations in annealing kinetics not captured by the annealing models (Flowers et al., 2009; Guenthner et al., 2013). For these samples, we increased individual grain error to 20% for the ZHe and/or AHe systems, altering no other input parameters, and reran the model. Twelve of the 22 samples with 20% ZHe and/or AHe grain error in HeFTy identified 100 t-T paths with a goodness of fit > 0.5 were recorded, and we designated these results as lower confidence (Table DR2). For ten samples, HeFTy's exploration of >100,000 possible time temperature paths failed to identify any good fit paths. We attribute this to a non-geologic discrepancy between thermochronolometric data, (e.g. helium implantation, mineral inclusions, U-Th rich grain boundary phases; Peyton et al., 2012; Murray et al., 2014) and these samples were excluded from further analysis.

We coded the temporal range of the onset of Neogene cooling by identifying two points (Table DR2; Figure DR2): 1) the time and temperature of the inflection point where the earliest possible cooling was required by the suite of 100 good fit paths (t_{cool}); and 2) the latest possible time where cooling was required by the model for the same temperature identified in point one. The mean of these two constraints is plotted in Figure 2B.

References

Christeleit, E.C., Brandon, M.T., and Shuster, D.L., 2017, Miocene development of alpine glacial relief in the Patagonian Andes, as revealed by low-temperature thermochronometry: Earth and Planetary Science Letters, v. 460, p. 152–163, doi: 10.1016/j.epsl.2016.12.019.

Donelick, R.A., 2005, Apatite Fission-Track Analysis: Reviews in Mineralogy and Geochemistry, v. 58, no. 1, p. 49-94, doi: 10.2138/rmg.2005.58.3.

Flowers, R.M., Ketcham, R.A., Shuster, D.L., and Farley, K.A., 2009, Apatite (U–Th)/He thermochronometry using a radiation damage accumulation and annealing model: Geochimica et Cosmochimica Acta, v. 73, no. 8, p. 2347-2365, doi: 10.1016/j.gca.2009.01.015.

Fosdick, J.C., Grove, M., Hourigan, J.K., and Calderón, M., 2013, Retroarc deformation and exhumation near the end of the Andes, southern Patagonia: Earth and Planetary Science Letters, v. 361, p. 504–517.

Georgieva, V., Melnick, D., Schildgen, T.F., Ehlers, T.A., Lagabrielle, Y., Enkelmann, E., and Strecker, M.R., 2016, Tectonic control on rock uplift, exhumation, and topography above an oceanic ridge collision: Southern Patagonian Andes (47°S), Chile: Tectonics, v. 35, no. 6, p. 1317-1341, doi: 10.1002/2016tc004120.

Guenthner, W.R., Reiners, P.W., Ketcham, R.A., Nasdala, L., and Giester, G., 2013, Helium diffusion in natural zircon: Radiation damage, anisotropy, and the interpretation of zircon (U-Th)/He thermochronology: American Journal of Science, v. 313, no. 3, p. 145-198, doi: 10.2475/03.2013.01.

Guillaume, B., Gautheron, C., Simon-Labric, T., Martinod, J., Roddaz, M., and Douville, E., 2013, Dynamic topography control on Patagonian relief evolution as inferred from low temperature thermochronology: Earth and Planetary Science Letters, v. 364, p. 157–167, doi: 10.1016/j.epsl.2012.12.036.

Haschke, M., Sobel, E.R., Blisniuk, P., Strecker, M.R., and Warkus, F., 2006, Continental response to active ridge subduction: Geophysical Research Letters, v. 33, doi: 10.1029/2006GL025972.
Ketcham, R.A., 2005, Forward and inverse modeling of low-temperature thermochronometry data: Reviews in Mineralogy and Geochemistry, v. 58, p. 275–314, doi: 10.2138/rmg.2005.58.11.
Ketcham, R.A., Carter, A., Donelick, R.A., Barbarand, J., and Hurford, A.J., 2007, Improved measurement of fission-track annealing in apatite using c-axis projection: American Mineralogist, v. 92, no. 5-6, p. 789-798, doi: 10.2138/am.2007.2280.
Murray, K.E., Orme, D.A., and Reiners, P.W., 2014, Effects of U–Th-rich grain boundary phases on apatite helium ages: Chemical Geology, v. 390, p. 135-151, doi: 10.1016/j.chemgeo.2014.09.023.
Peyton, S.L., Reiners, P.W., Carrapa, B., and DeCelles, P.G., 2012, Low-temperature thermochronology of the northern Rocky Mountains, western U.S.A.: American Journal of Science, v. 312, no. 2, p. 145-212, doi: 10.2475/02.2012.04.
Thomson, S.N., Hervé, F., and Stöckhert, B., 2001, Mesozoic-Cenozoic denudation history of the Patagonian Andes (southern Chile) and its correlation to different subduction processes: Tectonics, v. 20, p. 693–711.
Thomson, S.N., Brandon, M.T., Tomkin, J.H., Reiners, P.W., Vásquez, C., and Wilson, N.J., 2010, Glaciation as a destructive and constructive control on mountain building.: Nature, v. 467, no. 7313, p. 313–317, doi: 10.1038/nature09365.

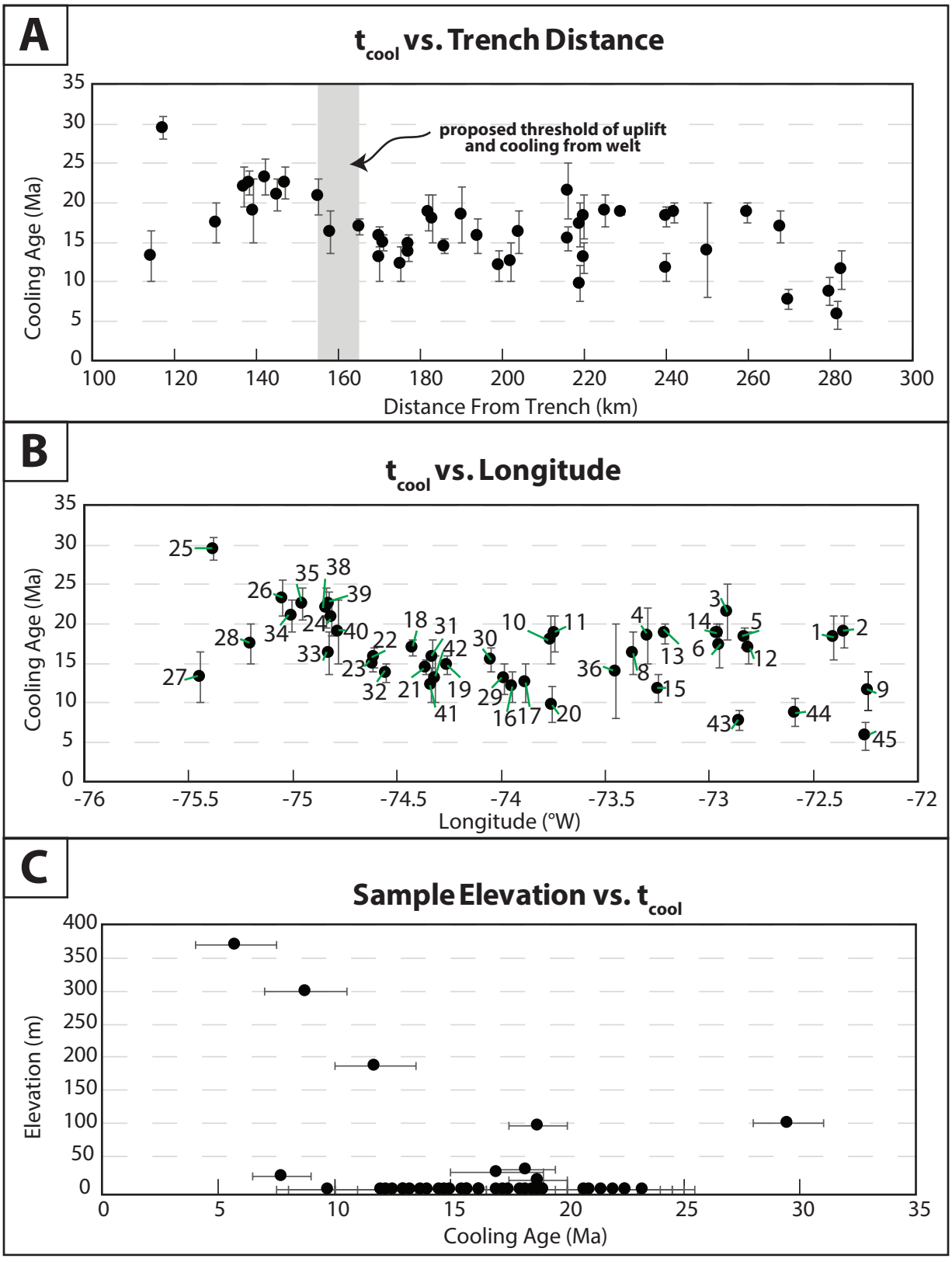
A
t_{cool} vs. Trench Distance
proposed threshold of uplift and cooling from welt
Cooling Age (Ma)
Distance From Trench (km)
B
t_{cool} vs. Longitude
Cooling Age (Ma)
Longitude (°W)
C
Sample Elevation vs. t_{cool}
Elevation (m)
Cooling Age (Ma)

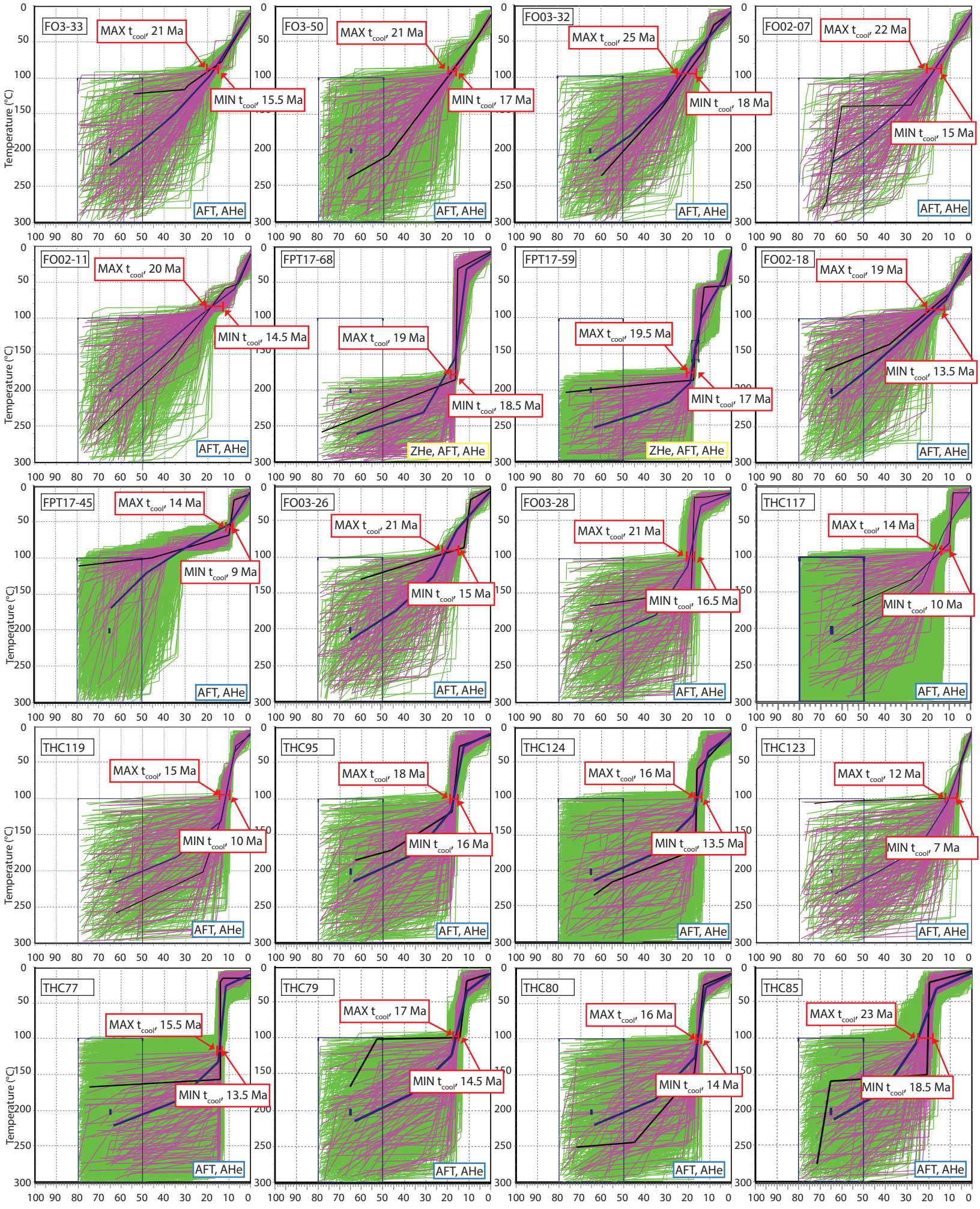
FO3-33
MAX t_cool, 21 Ma
MIN t_cool, 15.5 Ma
AFT, AHe
FO3-50
MAX t_cool, 21 Ma
MIN t_cool, 17 Ma
AFT, AHe
FO03-32
MAX t_cool, 25 Ma
MIN t_cool, 18 Ma
AFT, AHe
FO02-07
MAX t_cool, 22 Ma
MIN t_cool, 15 Ma
AFT, AHe
FO02-11
MAX t_cool, 20 Ma
MIN t_cool, 14.5 Ma
AFT, AHe
FPT17-68
MAX t_cool, 19 Ma
MIN t_cool, 18.5 Ma
ZHe, AFT, AHe
FPT17-59
MAX t_cool, 19.5 Ma
MIN t_cool, 17 Ma
ZHe, AFT, AHe
FO02-18
MAX t_cool, 19 Ma
MIN t_cool, 13.5 Ma
AFT, AHe
FPT17-45
MAX t_cool, 14 Ma
MIN t_cool, 9 Ma
AFT, AHe
FO03-26
MAX t_cool, 21 Ma
MIN t_cool, 15 Ma
AFT, AHe
FO03-28
MAX t_cool, 21 Ma
MIN t_cool, 16.5 Ma
AFT, AHe
THC117
MAX t_cool, 14 Ma
MIN t_cool, 10 Ma
AFT, AHe
THC119
MAX t_cool, 15 Ma
MIN t_cool, 10 Ma
AFT, AHe
THC95
MAX t_cool, 18 Ma
MIN t_cool, 16 Ma
AFT, AHe
THC124
MAX t_cool, 16 Ma
MIN t_cool, 13.5 Ma
AFT, AHe
THC123
MAX t_cool, 12 Ma
MIN t_cool, 7 Ma
AFT, AHe
THC77
MAX t_cool, 15.5 Ma
MIN t_cool, 13.5 Ma
AFT, AHe
THC79
MAX t_cool, 17 Ma
MIN t_cool, 14.5 Ma
AFT, AHe
THC80
MAX t_cool, 16 Ma
MIN t_cool, 14 Ma
AFT, AHe
THC85
MAX t_cool, 23 Ma
MIN t_cool, 18.5 Ma
AFT, AHe
Temperature (°C)
0 50 100 150 200 250 300
100 90 80 70 60 50 40 30 20 10 0

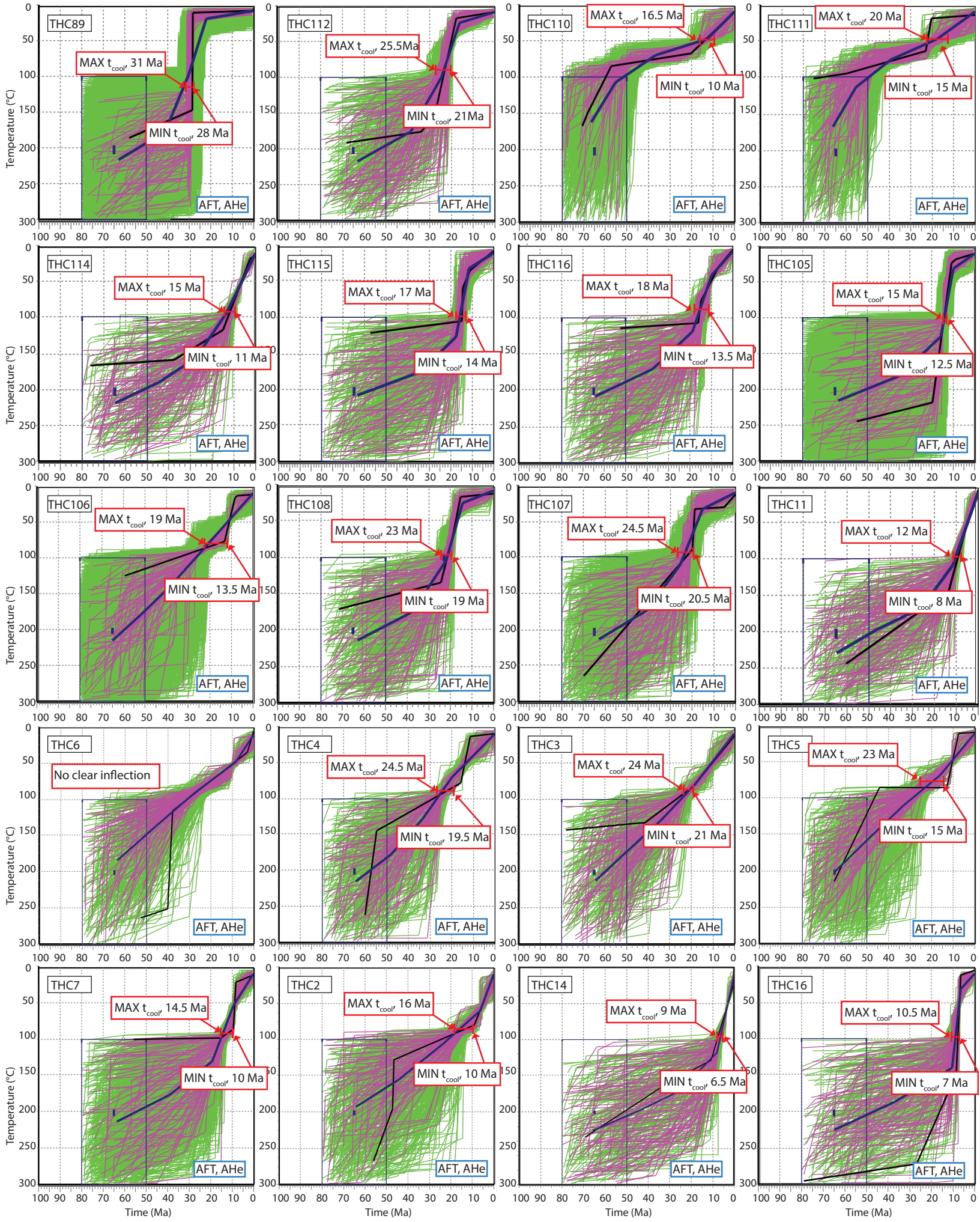
THC89
MAX t cool, 31 Ma
MIN t cool, 28 Ma
AFT, AHe
THC112
MAX t cool, 25.5Ma
MIN t cool, 21Ma
AFT, AHe
THC110
MAX t cool, 16.5 Ma
MIN t cool, 10 Ma
AFT, AHe
THC111
MAX t cool, 20 Ma
MIN t cool, 15 Ma
AFT, AHe
THC114
MAX t cool, 15 Ma
MIN t cool, 11 Ma
AFT, AHe
THC115
MAX t cool, 17 Ma
MIN t cool, 14 Ma
AFT, AHe
THC116
MAX t cool, 18 Ma
MIN t cool, 13.5 Ma
AFT, AHe
THC105
MAX t cool, 15 Ma
MIN t cool, 12.5 Ma
AFT, AHe
THC106
MAX t cool, 19 Ma
MIN t cool, 13.5 Ma
AFT, AHe
THC108
MAX t cool, 23 Ma
MIN t cool, 19 Ma
AFT, AHe
THC107
MAX t cool, 24.5 Ma
MIN t cool, 20.5 Ma
AFT, AHe
THC11
MAX t cool, 12 Ma
MIN t cool, 8 Ma
AFT, AHe
THC6
No clear inflection
AFT, AHe
THC4
MAX t cool, 24.5 Ma
MIN t cool, 19.5 Ma
AFT, AHe
THC3
MAX t cool, 24 Ma
MIN t cool, 21 Ma
AFT, AHe
THC5
MAX t cool, 23 Ma
MIN t cool, 15 Ma
AFT, AHe
THC7
MAX t cool, 14.5 Ma
MIN t cool, 10 Ma
AFT, AHe
THC2
MAX t cool, 16 Ma
MIN t cool, 10 Ma
AFT, AHe
THC14
MAX t cool, 9 Ma
MIN t cool, 6.5 Ma
AFT, AHe
THC16
MAX t cool, 10.5 Ma
MIN t cool, 7 Ma
AFT, AHe
Temperature (°C)
Time (Ma)

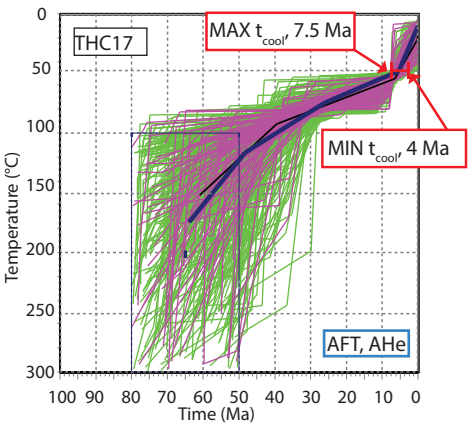
THC17
MAX t cool, 7.5 Ma
MIN t cool, 4 Ma
AFT, AHe
Temperature (°C)
Time (Ma)
0
50
100
150
200
250
300
100 90 80 70 60 50 40 30 20 10 0

DR 2. HeFTy Inverse Modeling Results

Example of data coding from HeFTy thermal model output